PAPER

Check for updates

Facile microwave-assisted synthesis of In$_2$O$_3$ nanocubes and their application in photocatalytic degradation of tetracycline

Gehong Zhang, [iD] *[a] Pinghai Lv,[b] Pingge Zhao,[a] Xuefu Yang,[a] Donghua Ma[a] and Yi Huang[a]

Novel In$_2$O$_3$ nanocube photocatalysts were successfully prepared by a facile microwave-assisted synthesis method. The obtained products are nano-sized with square corners and high crystallinity. The In$_2$O$_3$ nanocubes possessed high efficiency of electron–hole separation, resulting in high photocatalytic activities for the degradation of tetracycline under both visible light ($\lambda > 420$ nm) and full-range light irradiation (360–760 nm), the ratios of which are 39.3% and 61.0%, respectively. Moreover, the calculated positions of the CB and VB under our experimental conditions at the point of zero for In$_2$O$_3$ nanocubes are −0.60 V and +2.17 V, respectively. Note that the redox potentials of [O$_2$/·O$_2^-$] and [·OH/OH$^-$] are −0.33 V and +2.38 V, respectively, which means that the irradiated In$_2$O$_3$ nanocubes can reduce O$_2$ into ·O$_2^-$ without oxidizing OH$^-$ into ·OH. It can be concluded that ·O$_2^-$ and h$^+$ are the main active species of In$_2$O$_3$ in aqueous solution under visible light irradiation and full-range light irradiation.

1. Introduction

Antibiotics are a class of emerging contaminants in water because of the concern of their potential adverse effects on human health, mainly due to the increased bacterial resistance in the ecosystem. They have been found in a wide range of environmental samples including surface water, groundwater, wastewater and drinking water.[1–3] Tetracycline (TC), as a group of broad-spectrum antibacterial compounds, has afforded the medical profession a number of powerful antibiotics active against a wide range of human and animal pathogens.[4] Therefore, the removal of TC from the environment has become a mandatory issue.

Indium oxide (In$_2$O$_3$) is an n-type semiconductor. In$_2$O$_3$ has high conductivity and transparency, which makes it suitable for application in optoelectronics, gas sensors, photocatalysts and so on.[5,6] Many methods including organic solution synthetic routes, solvothermal methods, sol–gel methods, chemical vapor deposition, template routes, hot injection techniques, hydrothermal methods and microwave-assisted synthesis have been used to synthesize In$_2$O$_3$ with different morphologies.[6–13] Among these methods, microwave-assisted synthesis is a promising method for large-scale fabrication of nanomaterials, owing to its simplicity, low cost and environmental friendliness. However, the investigations by this technique on In$_2$O$_3$ have been quite limited.

In our paper, the precursors In(OH)$_3$ of In$_2$O$_3$ nanocubes are quickly synthesized with a microwave-assisted instrument. After annealing a In(OH)$_3$ precursor at 400 °C for 120 min, the In$_2$O$_3$ nanocubes are obtained. This process is simple, clean and more economical than conventional methods. In addition, In$_2$O$_3$ nanocubes exhibit high photocatalytic degradation ratio of TC under visible-light irradiation and full-range light irradiation, which are 39.3% and 61.0%, respectively. Furthermore, it might present a new opportunity of the removal of TC under visible-light irradiation.

2. Experimental

2.1 Materials

All the chemicals were purchased from Sigma-Aldrich Chemical Co., Ltd (China) and used as received without further purification. Deionized (DI) water was used throughout the whole experiment.

2.2 Characterization

The crystal structure of samples was determined by X-ray diffraction (XRD) method using Cu Kα radiation ($\lambda = 1.54178$ Å). Scanning electron microscopy (SEM) images were collected on an S-4800 field emission SEM (FESEM, Hitachi, Japan). The chemical composition of the samples was determined by scanning electron microscope-X-ray energy dispersion spectrum (SEM-EDX) with an accelerating voltage of 25 kV. Transmission electron microscopy (TEM) images were collected on an F20 S-TWIN electron microscope (Tecnai G2, FEI Co.), using

[a]School of Civil & Architecture Engineering, Xi'an Technological University, Xi'an, 710021, China

[b]State Grid Shaanxi Electric Power Research Institute, Xi'an, 710100, China

a 200 kV accelerating voltage. UV-vis diffused reflectance spectra of the samples were obtained from a UV-vis spectrophotometer (UV2550, Shimadzu, Japan), and $BaSO_4$ was used as a reflectance standard.

2.3 Catalyst preparation

In a typical preparation procedure, $In(NO_3)_3 \cdot 4.5H_2O$ (1 mmol) and urea (6 mmol) were dissolved in 100 mL deionized water. After stirring for 15 min, the obtained mixture was transferred into a quartz-glass container with capacity of 250 mL. The microwave reaction was carried out in a microwave reactor. The mixture was heated in the microwave reactor with the operating power of 800 W and working temperature of 100 °C for 120 min. After the container cooled to room temperature, the as-formed white precipitates were collected by centrifugation, washed with deionized water and absolute ethanol three times respectively, then dried in vacuum at 60 °C for 6 h. Finally, the obtained products were calcined in air at 400 °C for 2 h min with a heating rate 5 °C min^{-1} and cooled under air. The final products were In_2O_3 nanocubes.

2.4 Method of catalytic performance

The photodegradative reaction for TC was carried out at 298 K in a photochemical reactor under visible light. The photochemical reactor contains 0.1 g In_2O_3 photocatalyst and 20 mg L^{-1} of 100 mL TC solution. To determine the initial absorbance of samples, the reactor was kept into darkness for 30 min to reach absorption equilibrium. The photochemical reactor was irradiated with a 250 W xenon lamp which was located with a distance of 8 cm at one side of the containing solution. UV lights with wavelengths less than 420 nm were removed by a UV-cutoff filter in the visible-light-driven TC degradation experiment. The sampling analysis was conducted in 10 min interval. The photocatalytic degradation ratio (DR) was calculated by the following formula:

$$DR = \left(1 - \frac{A_i}{A_0}\right) \times 100\%$$

where A_0 is the initial absorbance of TC that reached absorption equilibrium, while A_i is the absorbance after the sampling analysis. The TC absorbance was measured by a UV-vis spectrophotometer with the maximum absorption wavelength at 355 nm.

3. Results and discussion

3.1 Characterization of the catalyst

The crystallographic phase purity of the as-synthesized In_2O_3 nanocubes were characterized by X-ray diffraction (XRD). As shown in Fig. 1, all characteristic peaks of In_2O_3 nanocubes can be readily indexed to the monoclinic phase of In_2O_3, which is in good agreement with the standard card (JCPDS no. 01-0929).

The morphology and crystalline structure of the as-obtained nanocubes are visualized by SEM and TEM images in Fig. 2. In the low-magnified SEM image (Fig. 2a), the obtained samples are formed as uniform nanocubes. According to the high-
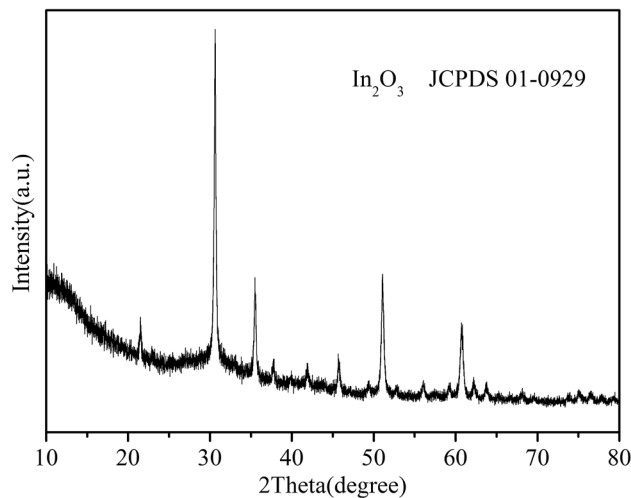

Fig. 1 XRD pattern of In_2O_3 nanocubes.

magnified SEM image (Fig. 2b), the picture reveals that the thickness of the cube structure (*ca.*100 nm) is within nanoscale level. The TEM image (Fig. 2c) suggests that the angle of the corner is nearly 90°, which further confirms the square character. Fig. 2d shows the SEM-EDX image of the as-prepared In_2O_3 samples, in which the signals of In and O can be clearly observed, which well coincides with the elementary composition of In_2O_3. The only impurity signal of Pt is ascribed to the substrate of the SEM-EDX analysis itself. The spectrum further indicates that the as-prepared In_2O_3 samples are pure.

3.2 Crystallization process

The possible formation mechanism of In_2O_3 nanocubes was divided into two processes.[14] Fig. 3a–c showed the morphology of the as-prepared samples with different microwave reaction time of 15 min, 30 min and 60 min, respectively. Fig. 3d shows the XRD patterns of the products obtained at 15 min, 30 min and 60 min, respectively. Firstly, the $In(OH)_3$ precursor with nanosheet-based was prepared by a simple hydrothermal route.
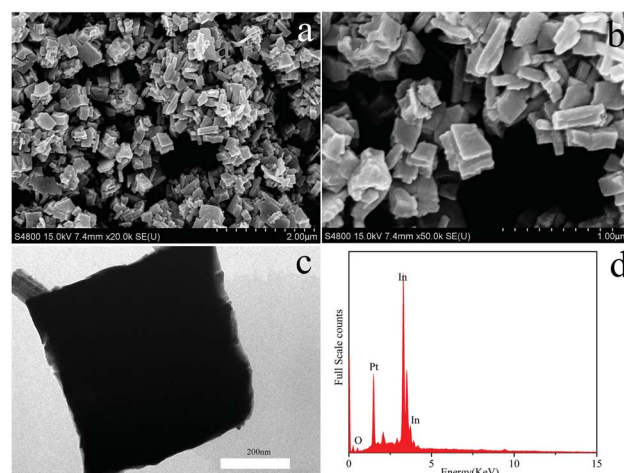

Fig. 2 SEM images in (a) low and (b) high magnifications; (c)TEM image and (d) SEM-EDX spectrum of In_2O_3 nanocubes.

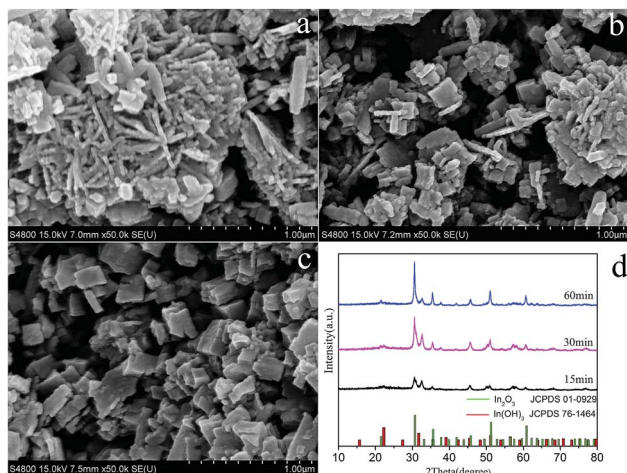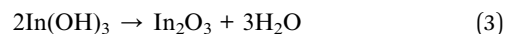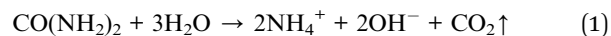Fig. 3 SEM images of obtained samples with different microwave reaction time: (a)15 min; (b) 30 min; (c) 60 min; (d) XRD patterns of the samples.

Then, In_2O_3 nanocubes were obtained under ambient pressure by the thermal decomposition of the $In(OH)_3$ precursor at 400 °C for 2 h. In order to understand the formation of In_2O_3 nanocubes, we studied the influence of time parameter on the morphology of products systematically. The influence of reaction time on the formation of In_2O_3 nanocubes was investigated as a variable while keeping all other reaction parameters the same. We found that the reaction time played an important role in controlling the morphology of the In_2O_3 nanostructures. When the reaction time is less than 15 min (Fig. 3a), the nanosheet-based products were observed. Combined with the XRD results (Fig. 3d), we consider that the composition of these nanosheet-based products are mainly $In(OH)_3$ but with a little of In_2O_3. When the reaction time reached 30 min, some sheet-like sheets formed gradually (Fig. 3b). Due to the ragged surface of these mutilated sheets, it can easily assume that the mutilated sheet-like structure is assembled by many $In(OH)_3$ nanosheets. Combined with the XRD patterns (Fig. 3d), we found that the corresponding peaks of In_2O_3 begin to strengthen, while characteristic peak of $In(OH)_3$ weaken gradually as the time went on. When the reaction time was increased to 60 min (Fig. 3c), the sheet structures begin to gather and nanocube-like aggregates appeared. Combined with the Fig. 3d, it is obvious that the intensity of In_2O_3 peaks are enhanced, but the $In(OH)_3$ composition is still subsistent in samples. Finally, as the reaction time was prolonged to 120 min (Fig. 2), the individual nanocubes disappeared completely and the well-defined nanocubes morphology appeared. From the XRD results, we can clearly see that the In_2O_3 phase begin to be predominant in the XRD pattern (Fig. 1) and the final product exhibits the complete square-sheet structure (Fig. 2a), and the composition of square sheets is pure In_2O_3 (Fig. 1).

According to above discussion, the possible reaction mechanism for the formation of In_2O_3 nanocubes refers to the similar literature data,[15,16] and the experimental results is as follows: First, $CO(NH_2)_2$ produce OH^- in the microwave-assisted synthesis process (reaction (1)). Then, these precursors and In^{3+} formed $In(OH)_3$ under the further stage of reaction (reaction (2)). Finally, they have transferred to In_2O_3 under a relatively longer period of thermal treatment (reaction (3)). Possible reaction formulas as followed:

$$CO(NH_2)_2 + 3H_2O \rightarrow 2NH_4^+ + 2OH^- + CO_2\uparrow \quad (1)$$

$$In^{3+} + 3OH^- \rightarrow In(OH)_3 \quad (2)$$

$$2In(OH)_3 \rightarrow In_2O_3 + 3H_2O \quad (3)$$

From the UV-vis absorption spectra (Fig. 4) of In_2O_3 nanocubes, the prepared In_2O_3 nanocubes have a strong absorption at *ca.* 448 nm, and the corresponding E_g of In_2O_3 nanocubes is 2.77 eV, resulting in the well response ability of In_2O_3 nanocubes to visible-light.[17]

The band edge positions of conduction band (CB) and valence band (VB) of In_2O_3 nanocubes can be determined by the following equation: $E_{CB} = \chi - E_e - 1/2E_g$, where E_{CB} is the conduction band edge potential, χ is the electronegativity of these semiconductor, E_e is the energy of free electrons on the hydrogen scale *ca.* 4.5 eV, E_g is the band gap of the semiconductor.

3.3 The kinetic study of photocatalytic degradationof TC

According to the Langmuir–Hinshelwood kinetics model,[18–22] the photocatalytic process of TC can be expressed as the following apparent first-order kinetics equation (eqn (4)).

$$\ln\left(\frac{C_0}{C}\right) = K_{app}t \quad (4)$$

where C is the concentration of solute remaining in the solution at irradiation time of t and C_0 is the initial concentration at $t = 0$. K_{app} denotes the degradation rate constant.

The apparent rate constant (K_{app}) has been chosen as the basic kinetic parameter for the different photocatalysts since it enables one to determine a photocatalytic activity independent
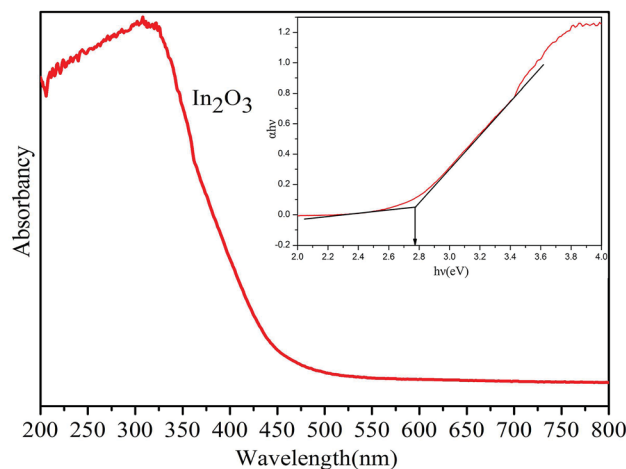

Fig. 4 UV-vis absorption spectrum of as-obtained In_2O_3 nanocubes.

of the previous adsorption period in the dark and the concentration of solute remaining in the solution.[22]

In order to further illustrate the photocatalytic reaction, the kinetic behavior is discussed. The photodegradation reaction kinetics of TC can be described by a Langmuir–Hinshelwood model according the report.[23] The decomposition of TC approximated the first order kinetic.

The variations in $\ln(C_0/C)$ as a function of irradiation times are given in Fig. 5. The calculated apparent rate constant K_{app} values for In_2O_3 under visible light and full range light irradiation respectively are given in Table 1.

3.4 Discussion of catalytic mechanism

As can be seen in the band structures of In_2O_3 nanocubes (Fig. 4), the calculated positions of CB and VB in our experimental condition at the point of zero for In_2O_3 nanocubes are −0.60 V and +2.17 V respectively. Note that the redox potentials of $[O_2/\cdot O_2^-]$ and $[\cdot OH/OH^-]$ are −0.33 V and +2.38 V,[24] respectively, which means the irradiated In_2O_3 nanocubes can reduce O_2 into $\cdot O_2^-$ without oxidizing OH^- into $\cdot OH$. Thus, the photocatalytic oxidation process of In_2O_3 nanocubes can be classified as the $\cdot O_2^-$ radical oxidation and h^+.

On the basis of the article,[14] we propose a plausible mechanism for the photodegradation of TC over the In_2O_3 nanocubes photocatalysts. The mechanistic pathway depicted in Scheme 1. As shown in Scheme 1, under the irradiation of visible light, the electron–hole pairs are excited from the VB of In_2O_3 nanocubes to its CB. The electron–hole pairs can then undergo further reactions with dissolved oxygen and water to form reactive
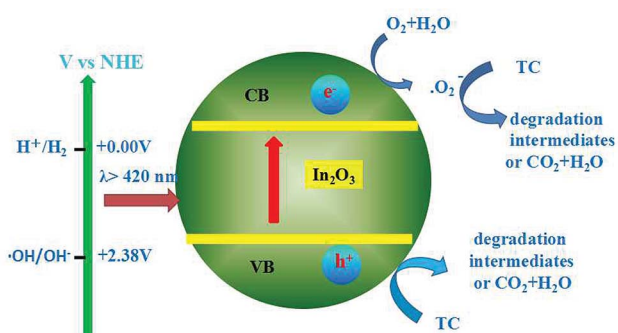
Scheme 1 Mechanistic transfer of electrons and holes on In_2O_3 nanocubes photocatalysts under visible light illumination.

radical species. The h^+ can oxidize TC directly, which are found to be the ruling active species in the photodegradation of TC. Moreover, O_2 in the water acts as an electron acceptor and generates $\cdot O_2^-$ species, which are found to be the active species in the photodegradation of TC.

3.5 Catalytic performance

To probe the potential application of In_2O_3 nanocubes in photocatalytic degradation of TC, we evaluated the photocatalytic degradation of TC by In_2O_3 nanocubes. As shown in Fig. 6, the DR (60 min) of In_2O_3 nanocubes are 39.3% and 61.0% under visible light and full range light irradiation respectively.

To evaluate the photostability of the as-prepared photocatalysts, the circulation experiments of the In_2O_3 for the photodegradation of TC was investigated. We have conducted four cycle experiments and obtained the photocatalytic degradation rate at the corresponding number of cycles. It was found that the degradation rate of the recycled products was only reduced by a small amount. As illustrated in Fig. 7, the photocatalytic activity of the In_2O_3 sample does not have noticeable change after the fourth recycles for the degradation of TC, in which the photocatalyst shows good photostability.
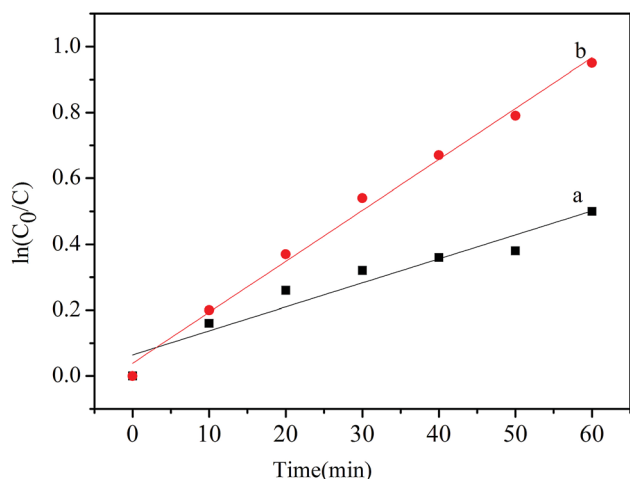

Fig. 5 Kinetics of the photocatalytic degradation of In_2O_3 nanocubes (a) under visible light and (b) under full-range light for 60 min.

Table 1 Apparent rate constant values for photo-degradation of the TC solution under visible light and full range light respectively in 60 min

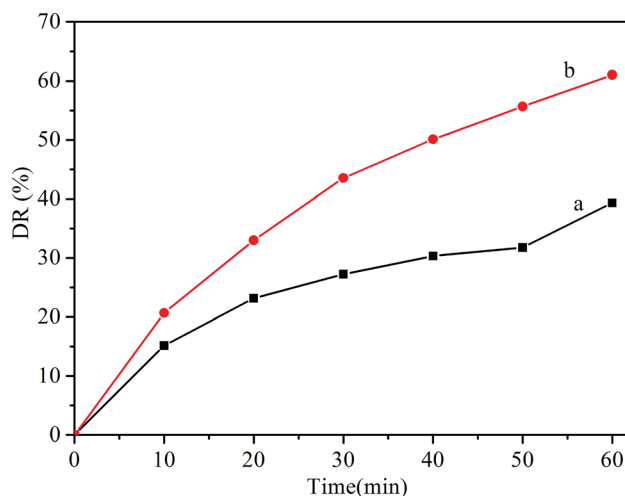| Condition	Visible light	Full range light
K_{app} (min^{-1})	0.0073	0.0154

Fig. 6 Photocatalytic degradation ratios of TC with In_2O_3 nanocubes under (a) visible-light and (b) full-range light irradiation for 60 min.
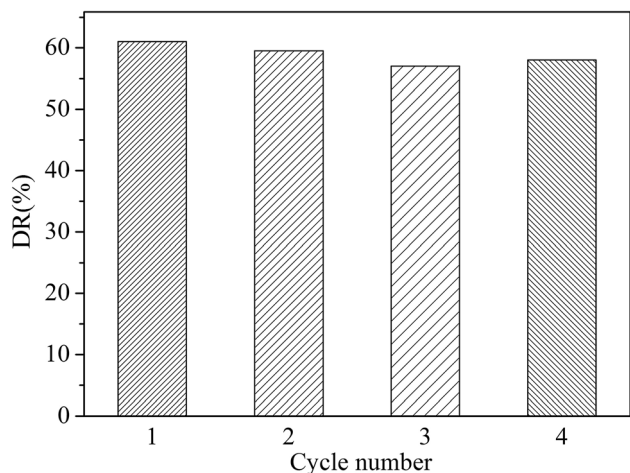
Fig. 7 Photodegradation rate of TC in solution for four cycles using In$_2$O$_3$ photocatalyst.

4. Conclusions

In summary, as-obtained In$_2$O$_3$ nanocubes exhibit visible-light-driven activity for photocatalytic degradation of TC. Our work highlights the facile and fast hydrothermal synthesis of In$_2$O$_3$ photocatalysts and exhibits visible-light-driven activity for photocatalytic degradation of TC.

Conflicts of interest

There are no conflicts to declare.

Acknowledgements

Notes and references

1 O. A. H. Jones, N. Voulvoulis and J. N. Lester, *Water Res.*, 2014, **36**, 5013.
2 K. D. Brown, J. Kulis, B. Thomson, T. H. Chapman and D. B. Mawhinney, *Sci. Total Environ.*, 2006, **366**, 772.
3 A. Pena, D. Chmielova, C. M. Lino and P. Solich, *J. Sep. Sci.*, 2007, **30**, 2924.
4 A. Pena, J. R. Albertgarcia, L. J. G. Silva, C. M. Lino and J. M. Calatayud, *J. Hazard. Mater.*, 2010, **179**, 409.
5 D. Caruntu, K. Yao, Z. X. Zhang, T. Austin, W. L. Zhou and C. J. O' Connor, *J. Phys. Chem. C*, 2010, **114**, 4875.
6 S. E. Lin and W. C. J. Wei, *J. Am. Ceram. Soc.*, 2006, **89**, 527.
7 J. Du, M. Yang, S. N. Cha, D. Rhen, M. Kang and D. J. Kang, *Cryst. Growth Des.*, 2008, **8**, 2312.
8 H. Kominami, T. Nakamura, K. Sowa, Y. Nakanishi, Y. Hatanaka and G. Shimaoka, *Appl. Surf. Sci.*, 1997, **113/114**, 519.
9 D. G. Shchukin and R. A. Caruso, *Chem. Mater.*, 2004, **16**, 2287.
10 W. Yin, M. Cao, S. Luo, C. Hu and B. Wei, *Cryst. Growth Des.*, 2009, **9**, 2173.
11 Z. Q. Liu, D. H. Zhang, S. Han, C. Li, T. Tang, W. Jin, X. L. Liu, B. Lei and C. W. Zhou, *Adv. Mater.*, 2013, **15**, 1754.
12 C. H. Liang, G. W. Meng, Y. Lei, F. Phillipp and L. D. Zhang, *Adv. Mater.*, 2010, **13**, 1330.
13 F. V. Motta, R. C. Lima, A. P. A. Marques, E. R. Leite, J. A. Varela and E. Longo, *Mater. Res. Bull.*, 2010, **45**, 1703.
14 M. M. Wu, C. Wang, Y. Zhao, L. S. Xiao, C. Zhang, X. Q. Yu, B. F. Luo, B. Hu, W. Q. Fan and W. D. Shi, *CrystEngComm*, 2015, **17**, 2336.
15 D. P. Dutta, M. Roy and A. K. Tyagi, *Dalton Trans.*, 2012, **41**, 10238.
16 G. H Zhang, X. Zhang, Y. Wu and W. D. Shi, *Micro Nano Lett.*, 2013, **8**, 177.
17 T. C. M. Muller, T. M. H. Tran, B. E. Pieters, A. Gerber, R. Carius and U. Rau, *Appl. Phys. Lett.*, 2013, **103**, 262108.
18 S. Valencia, F. Cataño, L. Rios, G. Restrepo and J. Marín, *Appl. Catal., B*, 2011, **104**, 300.
19 Z. Y. Lu, Y. Y. Luo, M. He, P. W. Huo, T. T. Chen, W. D. Shi, Y. S. Yan, J. M. Pan, Z. F. Ma and S. Y. Yang, *RSC Adv.*, 2013, **3**, 18373.
20 G. H. Zhang, W. S. Guan, H. Shen, X. Zhang, W. Q. Fan, C. Y. Lu, H. Y. Bai, L. S. Xiao, W. Gu and W. D. Shi, *Ind. Eng. Chem. Res.*, 2014, **53**, 5443.
21 C. Y. Lu, J. J. Dang, C. T. Hou, Y. J. Jiang and W. S. Guan, *Desalin. Water Treat.*, 2018, **104**, 250.
22 C. Zhao, M. Pelaezb, X. D. Duan, H. P. Deng, K. O'Shea, D. Fatta-Kassinos and D. D. Dionysiou, *Appl. Catal., B*, 2013, **134 −135**, 83–92.
23 J. F. Niu, S. Y. Ding, L. W. Zhang, J. B. Zhao and C. H. Feng, *Chemosphere*, 2013, **93**, 1–8.
24 M. R. Hoffmann, S. T. Martin, W. Choi and D. W. Bahnemann, *Chem. Rev.*, 1995, **95**, 69.